Pulmonary Lobe Segmentation with Level Sets

Alexander Schmidt-Richberg, Jan Ehrhardt, Matthias Wilms, René Werner and Heinz Handels

Institute of Medical Informatics, University of Lübeck, Lübeck, Germany

ABSTRACT

Automatic segmentation of the separate human lung lobes is a crucial task in computer aided diagnostics and intervention planning, and required for example for determination of disease spreading or pulmonary parenchyma quantification.

In this work, a novel approach for lobe segmentation based on multi-region level sets is presented. In a first step, interlobular fissures are detected using a supervised enhancement filter. The fissures are then used to compute a cost image, which is incorporated in the level set approach. By this, the segmentation is drawn to the fissures at places where structure information is present in the image. In areas with incomplete fissures (e.g. due to insufficient image quality or anatomical conditions) the smoothing term of the level sets applies and a closed continuation of the fissures is provided.

The approach is tested on nine pulmonary CT scans. It is shown that incorporating the additional force term improves the segmentation significantly. On average, 83% of the left fissure is traced correctly; the right oblique and horizontal fissures are properly segmented to 76% and 48%, respectively.

Keywords: level set segmentation, lung lobe segmentation

1. PURPOSE

Human lungs consist of five separate lobes, three in the right lung and two in the left. The lobes have individual bronchial and vascular systems and are functioning relatively independent from each other. A robust segmentation of the individual lobes is required for many applications in computer aided diagnostics and intervention. For example, it is clinically important to determine if affections in early stages are confined to single lobes, since the interlobular fissures stem the spread of diseases. Moreover, accurate segmentations are required to characterize and quantify malfunctions like residual pulmonary parenchyma.[1]

Lobe segmentation can be a very challenging task if images lack in quality or if anatomical anomalies occur. Therefore and due to its clinical relevance, a wide variety of approaches has been proposed. Most methods start from a segmentation of the interlobular fissures to separate the lobes. Wang et al.[2] propose a curve-growing process based on image features and atlas information to segment the fissures. Among others, Wiemker et al.[3] and Lassen et al.[4] propose a fissure enhancement based on the eigenvectors of the Hessian, similar to the vesselness measure. Van Rikxoort et al.[5] extend this approach to a supervised learning method based on the second order derivatives of the image. Most of these approaches perform well if images are of reasonably good quality. However, a detection of the fissures is often not sufficient to separate the lobes because fissures are incomplete for many subjects due to anatomical conditions or severe lung diseases.[6] Moreover, bad image quality and insufficient spatial resolution can cause fragmentary segmentations. This is addressed by Pu et al.[7] using an implicit surface fitting with different radial basis functions. Van Rikxoort et al.[8] instead propose an atlas-based completion of the fissures. A MAP-based sampling of fissure particles considering image features followed by a TPS interpolation is used by Ross et al.[9] Zhang et al.[10] use a fuzzy decision system considering image and atlas information for lobe segmentation. Ukil et al.[11] later apply Fast Marching Methods to complete fissures in projection images.

In this work, we propose an alternative approach based on level sets to segment the pulmonary lobes. Here, fissure-enhancing techniques are used to define an additional force term that draws the level set to the fissures. In image regions with insufficient fissure information, a smooth completion of the fissures is estimated by the level sets and thus closed objects are guaranteed.

Further author information: (Send correspondence to Alexander Schmidt-Richberg)
Alexander Schmidt-Richberg: E-mail: schmidt-richberg@imi.uni-luebeck.de, Telephone: +49 (0) 451 500 5645

Medical Imaging 2012: Image Processing, edited by David R. Haynor, Sébastien Ourselin,
Proc. of SPIE Vol. 8314, 83142V · © 2012 SPIE · CCC code: 0277-786X/12/$18 · doi: 10.1117/12.911378

2. METHODS

Level sets[12] have been proven to be a viable tool for various segmentation tasks in medical imaging. Due to the implicit formulation of the object boundary, level sets require no parametrization and are independent of a specific topology or dimensionality. Furthermore, object boundaries described by level sets are always closed. The formulation as an energy minimization task allows flexible adaption to specific problems.

In this work, an additional force term is proposed for the level set framework that attracts the segmentation to the fissures in the image. This force is designed to be neglectable in regions with high image contrast – e.g. near the boundaries of the lung – and high in a proximity to the fissures. The fact that level sets always represent closed objects is exploited in cases with incomplete fissures: In regions where neither image nor fissure information is present (be it due to lacking image quality or anatomical conditions), a smooth continuation is estimated by the level sets.

In the following, level sets are briefly introduced in section 2.1 including an extension to multi-object segmentation. A new fissure attraction force is proposed in section 2.1.2. Thereafter, an atlas-based initialization of the segmentation approach is examined and details of the implementation are given.

2.1 Level set segmentation

Let $I(\boldsymbol{x}) : \Omega \mapsto \mathbb{R}^d$ be an image with the domain $\Omega \subset \mathbb{R}^d$ and $\Sigma \subset \Omega$ an object in the image. Its boundary is represented implicitly as the zero-level curve of the level set function $\phi(\boldsymbol{x}) : \Omega \mapsto \mathbb{R}^d$. Here, ϕ is defined as the distance function to the boundary with $\phi(\boldsymbol{x}) < 0$, if $\boldsymbol{x} \in \Sigma$ and $\phi(\boldsymbol{x}) > 0$, if $\boldsymbol{x} \in \Omega \backslash \Sigma$. The optimal level set is determined by minimizing the energy functional

$$\mathcal{J}[\phi] := \mathcal{E}[I;\phi] \; + \; \alpha\mathcal{I}[\phi] \; . \tag{1}$$

The functional consists of two terms. The region-based external energy

$$\mathcal{E}[I;\phi] := -\int_\Omega (1 - H(\phi(\boldsymbol{x}))\log p_{in}(I(\boldsymbol{x}))) \; + \; H(\phi(\boldsymbol{x}))\log p_{out}(I(\boldsymbol{x})) \; d\boldsymbol{x}$$

integrates a-priori knowledge about intensity distributions p_{in} inside and p_{out} outside the lungs, respectively, and draws the segmentation to the lung boundaries. These distributions can be estimated by sampling lung and background voxels using a Parzen-Window strategy.[13] The Heaviside function H is used to describe inside and outside of the object.

The internal energy is defined as

$$\mathcal{I}[\phi] = \int_\Omega \nabla H(\phi(\boldsymbol{x})) \; d\boldsymbol{x}$$

and enforces a smooth surface. For the minimization with respect to the level set function, the Euler-Lagrange equation is derived and a gradient descent is performed according to

$$\frac{\partial\phi}{\partial t} = -\delta(\phi)\left(-\log\frac{p_{out}}{p_{in}} - \alpha\nabla\frac{\nabla\phi}{\|\nabla\phi\|}\right) \; .$$

Using this approach, one object of arbitrary topology can be segmented, e.g. the human lungs.

2.1.1 Level sets for multiple objects

To simultaneously segment the five pulmonary lobes, an extension of the level set framework has to be employed to handle multiple objects. Here, we follow the approach proposed by Brox et al.[14] The level set framework is extended by employing N functions $\phi_i, i = 0, \ldots, N-1$, each representing one object $\Sigma_i := \{\boldsymbol{x} : \phi_i(\boldsymbol{x}) < 0\}$. The energy (1) is minimized under the constraints $\bigcap_i \Sigma_i = \emptyset$ and $\bigcup_i \Sigma_i = \Omega$. The evolution equation then reads

$$\frac{\partial\phi_i}{\partial t} = -\delta(\phi)\left(e_i - \max_{H(\phi_j)<0, j\neq i}(e_j, e_i - 1)\right) \quad \text{with} \quad e_k := \log p_k - \frac{\alpha}{2}\nabla\frac{\nabla\phi_k}{\|\nabla\phi_k\|} \; . \tag{2}$$

In this formulation, e_i serves as a (mostly outwards-directed) force that is applied to the level set ϕ_i. The final update value is determined by a competition of this force and the maximal force of all adhering level set functions. The additional term $e_i - 1$ balances the force if no other object is in the proximity.

For lobe segmentation, we have $N = 6$ objects (background and five lobes) and set $p_0 := p_{out}$ and $p_i := p_{in}$ for $i = 1, \ldots, 5$. The final segmentation $S_i : \Omega \mapsto \{0, 1\}$ of lobe i is then $S_i := 1 - H(\phi_i)$.

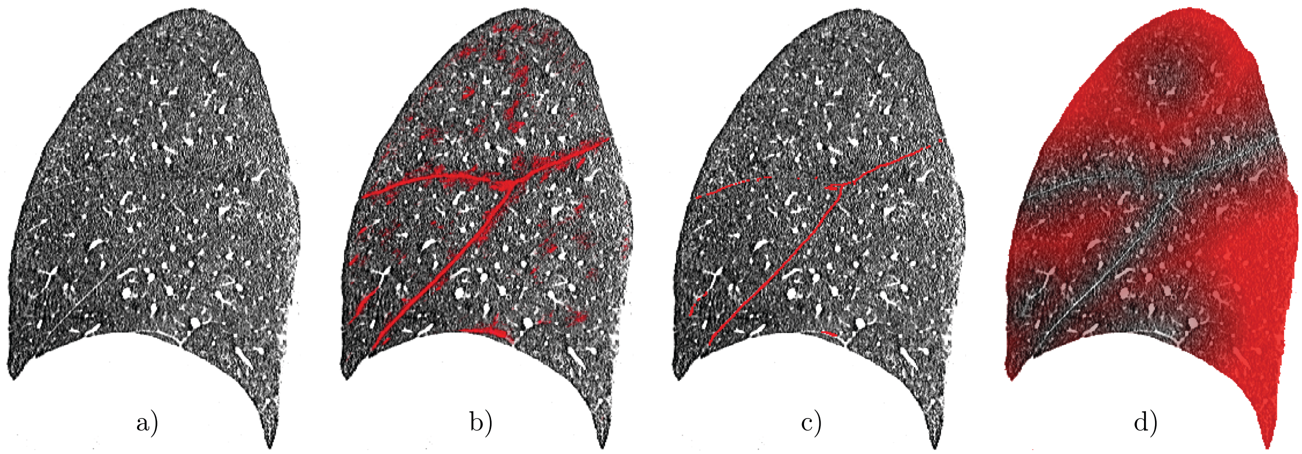

Figure 1. Computation of the cost image: a) the CT image I; b) the fissureness F image as output of the $k$nn classifier; c) the skeleton K of the post-processed fissureness image (dilated by one voxel to enhance visibility); d) the cost image C, which is incorporated in the force term.

2.1.2 Level sets with fissure-attraction forces

Using the model described above, only a smoothing is performed between two lobes because p_i equals p_j in these cases. Therefore, we define an additional term that draws the contour to the fissures.

In the first step, the interlobular fissures are segmented automatically. Since we want to prevent the level sets from being attracted by structures wrongly classified as fissures, we aim at a high specificity at the expense of sensitivity. Following previous studies,[15] we therefore chose the automatic supervised enhancement filter proposed by van Rikxoort et al.[5] The general idea is to sample intensity- and shape-based features at fissure- and non-fissure voxels of training images with known fissure segmentations and then train a statistical classifier to recognize the fissures in a test image.

Following van Rikxoort et al.,[5] a set of 57 features is identified. These are – each computed on four different scales with smoothing weight $\sigma = 1, 2, 4, 8$ – the grayvalue $(4 \cdot 1$ feature), the gradient components $(4 \cdot 3)$, gradient magnitude $(4 \cdot 1)$, the components of the Hessian matrix $(4 \cdot 6)$ and its eigenvalues $(4 \cdot 3)$ as well as the original grayvalue (1). A subset of these features is used to train a k-nearest neighbors ($k$nn) classifier with $k = 15$. Moreover, a two-phase strategy is applied; that means, the output of the first run of the classification is used as input for a second run. This procedure significantly reduces the influence of background noise.

The classifier provides a fissureness image $F : \Omega \mapsto \{0, \dots, k\}$ in which each voxel value indicates the number $m \leq k$ of the k nearest neighbors that were classified as fissure. Again aiming for high specificity, this image is then thresholded at $m \geq 14$ and a morphological closing followed by a connected-component analysis is performed to exclude small structures caused by noise.

The final goal is to define a cost image that is zero at the fissures and high apart from them. We therefore proceed by computing the topological skeleton K of the fissure segmentation and defining the cost image $C : \Omega \mapsto \mathbb{R}$ by $C(\boldsymbol{x}) := \sqrt{\mathrm{dist}_K(\boldsymbol{x})}$ where $\mathrm{dist}_K(\boldsymbol{x})$ is the Euclidean distance of point $\boldsymbol{x}$ to the skeleton K. With this, the force term in eq. (2) can be reformulated to incorporate a fissure-attraction force by

$$e_k := \log p_k - \frac{\alpha}{2} \nabla \frac{\nabla \phi_k}{\|\nabla \phi_k\|} - \frac{\beta}{2} \nabla \phi_k \cdot \nabla C \ . \tag{3}$$

The steps required for computing the cost image are illustrated in Figure 1.

2.2 Atlas-based initialization

The initialization of the level set segmentation is done by registration with a segmented lung atlas. To improve the results, a separate atlas is built for left and right lung using the following approach: First, the j images I_j of a training data set are registered to one arbitrarily chosen reference image using an affine pre-alignment of the lung surfaces followed by a non-linear diffeomorphic registration,[16] yielding the transformation $\varphi_j^{(0)}$. Registration

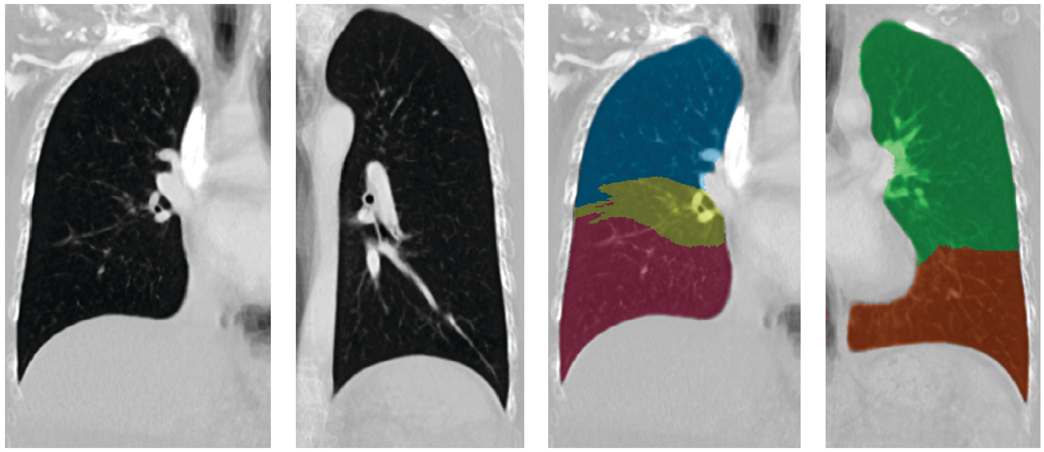

Figure 2. The mean intensity and shape atlas $\bar{I}^{(3)}$ of the left and right lung and the corresponding lobe segmentations.

is done using lung masks, that means only the inside of the lung is matched. The images are then transformed to the reference frame by $I_j \circ \varphi_j^{(0)}$ and the mean image $\bar{I}^{(0)}$ is computed.

To avoid a bias due to the choice of the reference frame, an iterative approach proposed by Guimond et al.[17] is pursued. For this, the mean transformation $\bar{\varphi}^{(0)}$ is computed and its inverse used to transform the mean image. Then, registration of all images is repeated with $\bar{I}^{(0)} \circ (\bar{\varphi}^{(0)})^{-1}$ as reference image. This approach is iterated until the average transformation converges against the identity and the mean shape and intensity atlas $\bar{I}^{(n)}$ is obtained after n iterations. Finally, the lobe segmentations of the images I_j are also transferred to the coordinate system of the atlas and then combined using the standard vote rule to represent a segmentation of the mean shape and intensity image.

An initialization for the segmentation of an unseen test image can then be generated by registering that image to the atlas and transferring the atlas segmentation to the image.

2.3 Image data and evaluation procedure

The presented approach for lobe segmentation was tested on a set of nine thoracic normal dose CT images I_j, $j \in \{1, \ldots, 9\}$ (120 kVp, 450-750 mAs, $0.79 \times 0.79 \times 0.7$ mm spacing). For each image, manual fissure and lobe segmentations were provided for training/atlas generation and evaluation.

For fissure segmentation, 1000 fissure- and background voxels each were sampled per training image. Moreover, a leave-one-out strategy was applied, that means to segment image I_j features were sampled in each image I_l with $j \neq l$, resulting in 16k samples in total.

It has to be noted that the atlas was not generated using a leave-one-our strategy but considering all nine images. This was done mainly for computational reasons but since the atlas is only used for initialization and bearing in mind the observations made in Ehrhardt et al.,[18] we consider the resulting bias to be neglectable. Atlas and corresponding lobe segmentation are illustrated in Figure 2.

The segmentation approach is implemented using *sparse field level sets*.[19] Moreover, a multi-level strategy is applied to improve both segmentation results and computational efficiency. The parameters were determined empirically and used unaltered for all images: $\tau = 0.5$, $\alpha = 1.0$, $\beta = 0.5$. A total of 600 iterations were performed on two resolution levels.

For evaluation, three segmentations S are compared with the manual reference segmentation M: the initialization S^{Init} as described in section 2.2, the standard level set segmentation S^{Std} without the additional force term (eq. (1)) and the proposed segmentation approach for lobe segmentation S^{Lobe}, eq. (3). Segmentation quality is quantified separately for each lobe i using the Dice coefficient:

$$Dice(M_i, S_i) := 2\, \frac{|\mathrm{supp}(M_i) \cap \mathrm{supp}(S_i)|}{|\mathrm{supp}(M_i)| + |\mathrm{supp}(S_i)|}\ ,$$

where supp denotes the support of the segmentation.

Since the Dice coefficient is difficult to interpret due to the varying size of the lobes, an additional metric

Metric	Lobe/Fissure	S^{Init}	S^{Std}	S^{Lobe}
Dice	left superior	0.94 ± 0.02	0.94 ± 0.02	0.98 ± 0.00
	left inferior	0.94 ± 0.03	0.94 ± 0.02	0.98 ± 0.01
	right superior	0.93 ± 0.02	0.94 ± 0.02	0.97 ± 0.02
	right middle	0.78 ± 0.06	0.78 ± 0.06	0.83 ± 0.13
	right inferior	0.92 ± 0.02	0.92 ± 0.02	0.93 ± 0.06
	mean	0.90 ± 0.02	0.90 ± 0.02	0.94 ± 0.04
Fiss	left	0.25 ± 0.22	0.24 ± 0.21	0.83 ± 0.07
	right oblique	0.25 ± 0.16	0.24 ± 0.16	0.76 ± 0.13
	right horizontal	0.24 ± 0.12	0.23 ± 0.12	0.48 ± 0.24

Table 1. Quantitative evaluation results for the three segmentations, averaged over all nine data sets: the initial segmentation S^{Init}, the standard level set segmentation S^{Std} and the level set segmentation with additional lobe force S^{Lobe}.

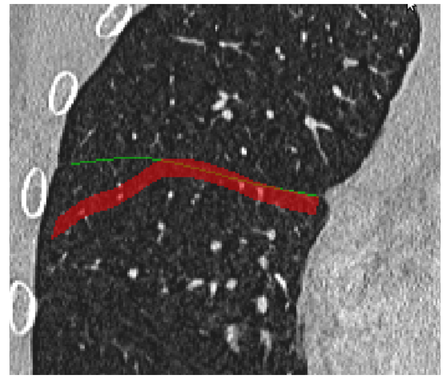

Figure 3. Illustration of how the metric $Fiss$ is calculated. $Fiss$ is the proportion of $B(M)$ (green) that lies in $B^+(S)$ (red).

is introduced similar to that proposed by Murphy et al.[20] It aims at quantifying the proportion of the lobe boundaries that are successfully traced in the segmentation result. Let $B(S)$ be the set of voxels of segmentation S that lie at the boundary between two lobes. To incorporate some tolerance, this region is expanded by ± 3 voxels in z-direction and denoted by B^+. The proportion of correctly segmented lobe boundaries can then be quantified by

$$Fiss(M, S) := \frac{|\{\boldsymbol{x} : \boldsymbol{x} \in B(M) \wedge \boldsymbol{x} \in B^+(S)\}|}{|\{\boldsymbol{x} : \boldsymbol{x} \in B(M)\}|} \, .$$

This approach is illustrated in Figure 3.

3. RESULTS AND DISCUSSION

Exemplary results of the presented approach for lobe segmentation are shown in Figure 4. The atlas-based initialization (second column) depicts the approximate anatomy of the lungs but lobe boundaries are often remote from the actual fissures. Using the multi-object level set approach without additional force term (third column), lung boundaries are segmented precisely but in the inside of the lung only the smoothing condition applies. Adding the presented force term however causes an attraction of the lobe boundaries to the fissures (last column). The strength of the approach becomes apparent in areas with gaps in the detected fissure segmentations: Due to the formulation of the cost image as distance map, the level set automatically finds the shortest connection between the fissure segments.

Quantitative results are given in Table 1. In all cases, lobe segmentations were considerably enhanced using the presented fissure attraction force. The improvement is also statistically significant ($p < 0.005$) for all metrics except the Dice coefficient of the right superior and middle lobe. It is also apparent that left lobes are segmented considerably better (83% of the boundary is traced correctly) than the three right lobes (76% and 48%). This can be explained by the risk that the level set is attracted by the wrong fissure if the initialization is considerably apart. Moreover, detection of the right horizontal fissure is often inferior to the other two fissures.

It can be observed that segmentation quality mainly depends on two aspects of the algorithm: the calculation of the cost image and the initialization. Fissure segmentation is sensitive to image quality and may therefore be insufficient for images with low resolution or reconstruction artifacts. While gaps in the fissures can be compensated by the level set formulation, it may impair the segmentation if a whole part of a fissure is missing. This is demonstrated in Figure 5 (left), where the boundary is attracted by the oblique fissure because the horizontal fissure is detected incompletely. The inverse problem is caused if structures are falsely classified as fissure and therefore cause an attraction of the segmentation (Figure 5, right). These limitations are evident especially in areas where the initialization is unsatisfying and apart from the fissures. Here, the segmentation may be attracted either by the wrong fissure or by other structures or noise in the images falsely classified as fissures.

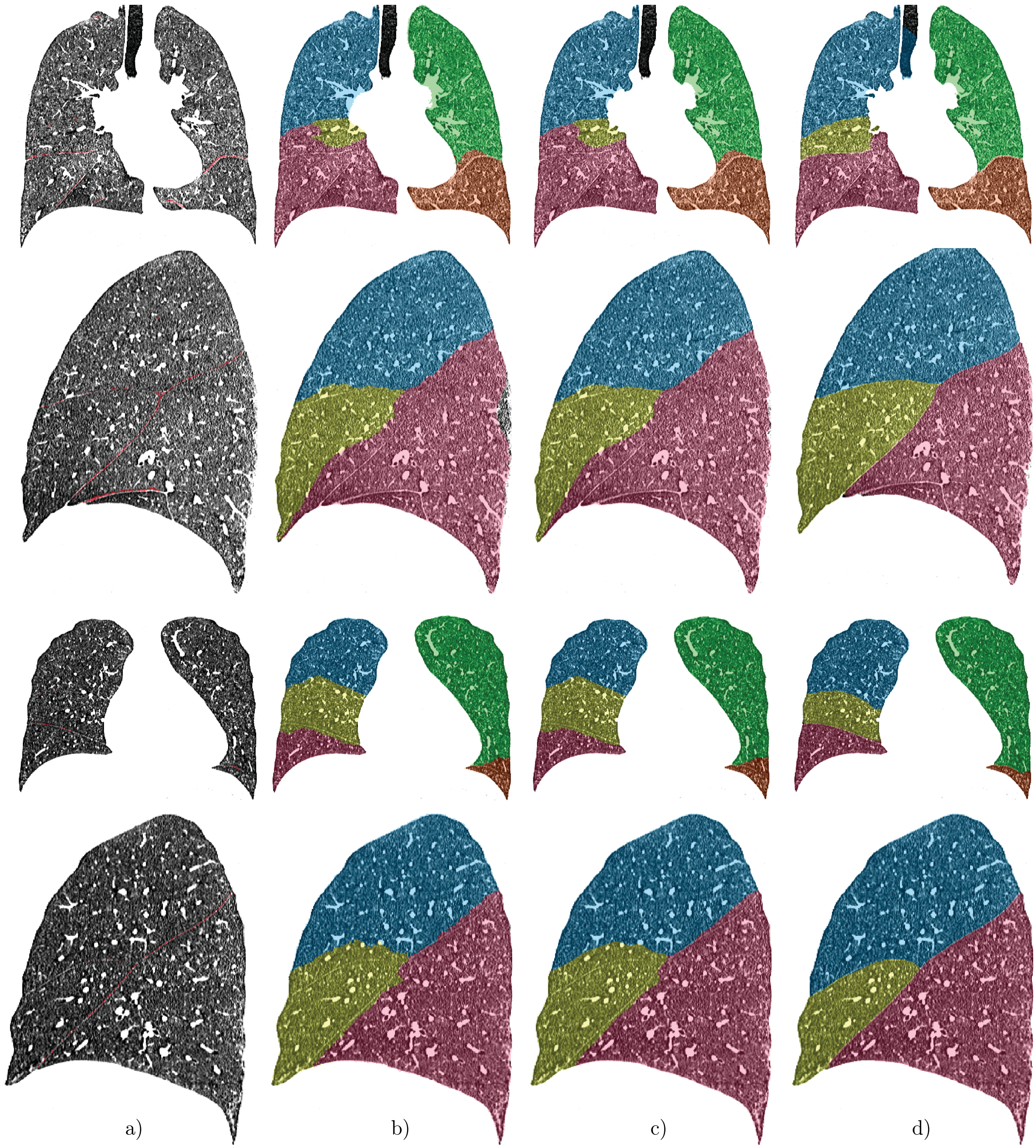

Figure 4. From left to right: a) the image I with the skeleton K of the fissure segmentation as red overlay; b) the atlas-based initialization of the segmentation; c) the result of the standard level set segmentation; d) the result of the level set segmentation with additional lobe force.

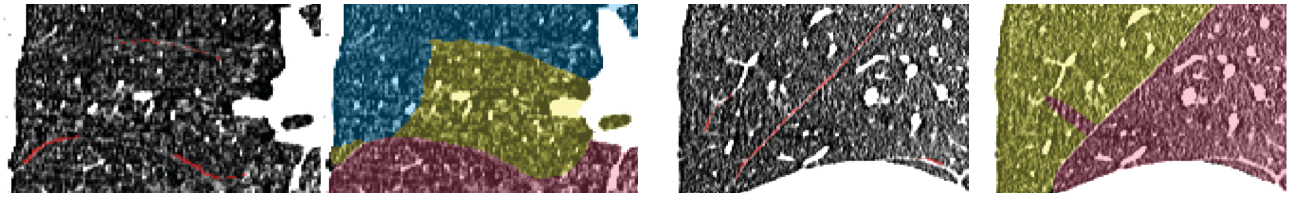

Figure 5. Limitations of the presented approach: Incomplete fissure segmentations (left) or structures incorrectly classified as fissures (right) can impair the segmentation result.

4. CONCLUSION

In this work, a novel approach for pulmonary lobe segmentation based on multi-region level sets is presented. Fissure information is extracted from the image using a supervised enhancement filter. The information is incorporated in the level set framework in form of a new force term.

It is shown that the presented method is capable of segmenting the pulmonary lobes. The approach performs best for the left lung where on average a part of 83% of the interlobular fissure was precisely detected. In the right lung, only 76% and 48% of oblique and horizontal fissure were traced correctly because they are close to each other and the segmentation is in risk of being attracted by the wrong one. These results show that the method depends on a reasonably good fissure detection and initialization, which may suffer from insufficient image quality. In future work, this problem can be addressed by consideration of additional anatomical information like the vasculature to distinguish between the lobes.

ACKNOWLEDGMENTS

This work is supported by the German Research Foundation DFG (EH 224/3-1). The authors would also like to thank Dr. Attila Kovac, University Medical Center Schleswig-Holstein, for providing the image data.

REFERENCES

[1] Sluimer, I., Schilham, A., Prokop, M., and van Ginneken, B., "Computer Analysis of Computed Tomography Scans of the Lung: A Survey," *IEEE Trans Med Imag* **25**(4), 385–405 (2006).

[2] Wang, J., Betke, M., and Ko, J. P., "Pulmonary fissure segmentation on CT," *Med Image Anal* **10**(4), 530–547 (2006).

[3] Wiemker, R., Bülow, T., and Blaffert, T., "Unsupervised extraction of the pulmonary interlobar fissures from high resolution thoracic CT data," in [*Proc CARS*], 1121–1126 (2005).

[4] Lassen, B., Kuhnigk, J.-M., Friman, O., Krass, S., and Peitgen, H.-O., "Automatic Segmentation of Lung Lobes in CT Images Based on Fissures, Vessels, and Bronchi," in [*Proc IEEE Int Symp Biomed Imaging*], 560–563 (2010).

[5] van Rikxoort, E. M., van Ginneken, B., Klik, M., and Prokop, M., "Supervised Enhancement Filters: Application to Fissure Detection in Chest CT Scans," *IEEE Trans Med Imag* **27**(1), 1–10 (2008).

[6] Aziz, A., Ashizawa, K., Nagaoki, K., and Hayashi, K., "High Resolution CT Anatomy of the Pulmonary Fissures," *J Thorac Imaging* **19**(3), 186–191 (2004).

[7] Pu, J., Zheng, B., Leader, J. K., Fuhrman, C., Knollmann, F., Klym, A., and Gur, D., "Pulmonary Lobe Segmentation in CT Examinations Using Implicit Surface Fitting," *IEEE Trans Med Imag* **28**(12), 1986–1996 (2009).

[8] van Rikxoort, E. M., Prokop, M., de Hoop, B. J., Viergever, M. A., Pluim, J. P. W., and van Ginneken, B., "Automatic Segmentation of Pulmonary Lobes Robust against Incomplete Fissures," *IEEE Trans Med Imag* **29**(6), 1286–1296 (2010).

[9] Ross, J. C., San José Estépar, R., Kindlmann, G., Díaz, A., Westin, C.-F., Silverman, E. K., and Washko, G. R., "Automatic Lung Lobe Segmentation Using Particles, Thin Plate Splines, and Maximum a Posteriori Estimation," in [*Med Image Comput Comput Assist Interv*], 163–171 (2010).

[10] Zhang, L., Hoffman, E. A., and Reinhardt, J. M., "Atlas-Driven Lung Lobe Segmentation in Volumetric X-Ray CT Images," *IEEE Trans Med Imag* **25**(1), 1–16 (2006).

[11] Ukil, S. and Reinhardt, J. M., "Anatomy-Guided Lung Lobe Segmentation in X-Ray CT Images.," *IEEE Trans Med Imag* **28**(2), 202–214 (2009).

[12] Osher, S. and Sethian, J. A., "Fronts Propagating with Curvature-Dependent Speed: Algorithms Based on Hamilton-Jacobi Formulations," *J Comp Phys* **79**, 12–49 (1988).

[13] Schmidt-Richberg, A., Handels, H., and Ehrhardt, J., "Integrated segmentation and non-linear registration for organ segmentation and motion field estimation in 4D CT data," *Methods Inf Med* **48**(4), 344–349 (2009).

[14] Brox, T. and Weickert, J., "Level Set Segmentation with Multiple Regions," *IEEE Trans Image Process* **15**(10), 3213–3218 (2006).

[15] Schmidt-Richberg, A., Ehrhardt, J., Werner, R., Wilms, M., and Handels, H., "Evaluation of Algorithms for Lung Fissure Segmentation in CT Images," in [*Proc BVM*], (2012). (in press).

[16] Schmidt-Richberg, A., Ehrhardt, J., Werner, R., and Handels, H., "Diffeomorphic Diffusion Registration of Lung CT Images," in [*Medical Image Analysis for the Clinic: A Grand Challenge, Workshop proceedings from MICCAI 2010*], 55–62 (2010).

[17] Guimond, A., Meunier, J., and Thirion, J.-P., "Automatic Computation of Average Brain Models," in [*Med Image Comput Comput Assist Interv*], 631–640 (1998).

[18] Ehrhardt, J., Werner, R., Schmidt-Richberg, A., and Handels, H., "A Statistical Shape and Motion Model for the Prediction of Respiratory Lung Motion," in [*Proc SPIE*], (2010).

[19] Whitaker, R. T., "A Level-Set Approach to 3D Reconstruction from Range Data," *Int J Comput Vis* **29**(3), 203–231 (1998).

[20] Murphy, K., van Ginneken, B., Reinhardt, J. M., Kabus, S., Ding, K., Deng, X., et al., "Evaluation of Registration Methods on Thoracic CT: The EMPIRE10 Challenge," *IEEE Trans Med Imag* **30**(11), 1901–1920 (2011).